Synthesis and structural characterization of new phosphinooxazoline complexes of iron

Sergey L. Sedinkin, Nigam P. Rath, Eike B. Bauer *

University of Missouri – St. Louis, Department of Chemistry and Biochemistry, One University Boulevard, St. Louis, MO 63121, USA

ABSTRACT

The first phosphinooxazoline chelate complexes of iron were synthesized, and their structural and electronic properties were studied.

The known phosphinooxazolines 2-(2-(diphenylphosphino)phenyl)-4,5-dihydrooxazole (**7a**), 2-(2-(diphenylphosphino)phenyl)-4,4-dimethyl-4,5-dihydrooxazole (**7b**), (*S*)-4-benzyl-2-(2-(diphenylphosphino)phenyl)-4,5-dihydrooxazole (**7e**) and (*R*)-2-(2-(diphenylphosphino)phenyl)-4-phenyl-4,5-dihydrooxazole (**7f**) were synthesized by a modified three step literature procedure with improved 67–60% overall yields. The new electronically tuned phosphinooxazolines 2-(5-bromo-2-(diphenylphosphino)phenyl)-4,4-dimethyl-4,5-dihydrooxazole (**7c**), 3-(4,4-dimethyl-4,5-dihydrooxazol-2-yl)-4-(diphenylphosphino)-*N,N*-dimethylaniline (**7d**) and 2-(2-(diphenylphosphino)-3-(trifluoromethyl)-phenyl)-4,4-dimethyl-4,5-dihydrooxazole (**7g**) were synthesized in three to six steps with 59–29% overall yields. Reaction of **7a–f** with CpFe(CO)$_2$I (110 °C, 2 h, toluene) gave the iodide salts of the new iron phosphinooxazoline complexes [CpFe(CO)(**7a–f**)]$^+$ in 87–21% yield. The new complexes were characterized by X-ray and the molecular structures confirm the octahedral coordination geometry and the half-sandwich structure about the iron center. The impact of different oxazoline ligands on the steric and electronic properties of their iron complexes was determined by analysis of selected bond lengths, $v_{C\equiv O}$ stretching frequency and the oxidation potentials of the ligands and the iron complexes.

© 2008 Elsevier B.V. All rights reserved.

1. Introduction

Phosphinooxazolines (PHOX, **1** in Fig. 1) [1] are an efficient, non-C_2-symmetric, bidentate, P,N chelating ligand class first described by Pfaltz [2a], Helmchen [2b] and Williams [2c]. Their development was inspired by Crabtree's catalyst [(cod)Ir(PCy$_3$)(py)][PF$_6$] (**2**), featuring a phosphine and a pyridine ligand in its coordination sphere (Fig. 1) [3]. Crabtree's catalyst is highly active in catalytic hydrogenation reactions, particularly for highly substituted olefins. PHOX ligands were successfully employed in transition metal catalyzed asymmetric reactions for such conversions as allylic alkylations [2b,4], allylation reactions [5], Heck reactions [6], hydrogenations of olefins [7] and ketones [8], transfer hydrogenation of ketones [9], Diels–Alder reactions [10], and conjugate addition to enones [11]. The efficiency of the PHOX ligands is in part ascribed to their ability to create distinguishable coordination sites trans to the phosphorus and nitrogen donors, enhancing selectivities [1a,12]. Modifications of the PHOX ligands **1** are mainly undertaken at the carbon atom α to the oxazoline nitrogen [9,13] and at the two aryl groups on phosphorus [4b,9,13].

Mainly iridium, rhodium, ruthenium and palladium are employed as metal centers in the catalytic reactions described above. Iron, however, is typically not the first choice when it comes to the development of new catalyst systems. However, iron has a number of advantages over other metals. It is cheap, non-toxic, environmentally friendly and abundant. Consequently, iron is increasingly investigated as an alternative for established transition metal catalyzed reactions such as C–C, C–N and C–O bond forming as well as oxidation and reduction reactions [14]. Phosphines and nitrogen-based ligands are the most prevalent in iron catalyzed reactions. However, we are not aware of the application of iron PHOX complexes in catalysis. Braunstein reported heterobimetallic iron copper complexes, where the two metal centers are bridged by PHOX ligands [15]. These bimetallic complexes are catalytically active in Diels–Alder and cyclopropanation reactions, but only the phosphorus atom is coordinated to the iron center.

We were interested to determine if iron can form stable chelate complexes with PHOX ligands. To the best of our knowledge such complexes are not known to date. We were also interested whether the electronic properties of the iron center could be fine tuned via variation of the substitution pattern of the PHOX ligand. Insights into the relationship between the structure of the ligand

* Corresponding author.
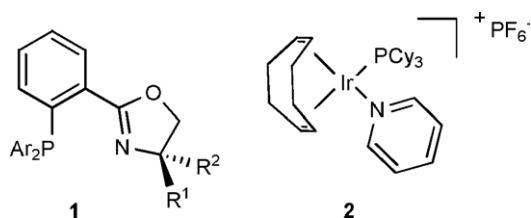*E-mail address:* bauere@umsl.edu (E.B. Bauer).

Fig. 1. PHOX ligands (1) and Crabtree's catalyst (2).

and the properties of the corresponding iron complexes are helpful in the development of new iron PHOX based catalyst systems.

Herein, we describe the first examples of iron PHOX chelate complexes. We synthesized a range of PHOX ligands varying in their electronic and steric properties. Iron complexes of these PHOX ligands were synthesized and structurally characterized, and the impact of the ligand structure on the steric and the electronic properties of the complexes were investigated.

2. Results

2.1. Synthesis of new phosphinooxazoline ligands

First, a set of sterically and electronically tuned phosphinooxazoline ligands was synthesized. We sought electronic tuning by incorporating different functional groups at the phenyl connected to the oxazoline, while steric tuning was incorporated with substituents at the carbon in the position α to the nitrogen of the oxazoline (Fig. 1).

Several approaches to oxazoline ring systems are known [16]. They typically utilize aromatic carboxylic acids or their synthetic equivalents (such as acid chlorides or nitriles) and β-aminoalcohols as starting materials. One pot syntheses from these reagents catalyzed by $ZnCl_2$ are known [2c,17], but harsh conditions are required (such as refluxing chlorobenzene) and yields are typically moderate. However, some two-step procedures from these starting materials often provide a more efficient pathway to oxazolines, and one pathway is shown in Scheme 1 [4b,18]. During our studies we found, that this two-step procedure was indeed more efficient than the one step processes, leading to higher overall yields of the corresponding PHOX ligands, which is in agreement with previous reports [18].

Accordingly, the known PHOX ligands 7a, 7b, (S)-7e and (R)-7f were synthesized via this standard method following modified literature procedures [18], as shown in Scheme 1. The benzoic acids (3) were first converted to the acid chlorides (4), utilizing oxalyl chloride $(COCl)_2$, which were then reacted with the appropriate aminoalcohol to give the amides 5a,b,e,f. The amides were cyclized to the oxazolines 6a,b,e,f with p-toluenesulfonic acid chloride (TsCl), and finally, in a nucleophilic aromatic substitution, the fluoride substituent was exchanged for PPh_2 using commercial $KPPh_2$. Some of the overall yields were improved over known literature procedures [18], and full experimental details for these syntheses may be found in the Supplementary material.

Next, electronic tuning via placing substituents at the phenyl core was accomplished. To obtain information about the influence of halogen substituents, commercial 2-fluorobenzoic acid was selectively monobrominated by electrophilic aromatic substitution. A mixture of $NaBrO_3/H_2SO_4$ was employed as the bromination agent, and 5-bromo-2-fluorobenzoic acid (3c) was obtained as white crystals in 88% yield (Eq. (1)). This material was further elaborated to the corresponding PHOX ligand 7c by the standard reaction sequence shown in Scheme 1 in 43% overall yield from 3c.
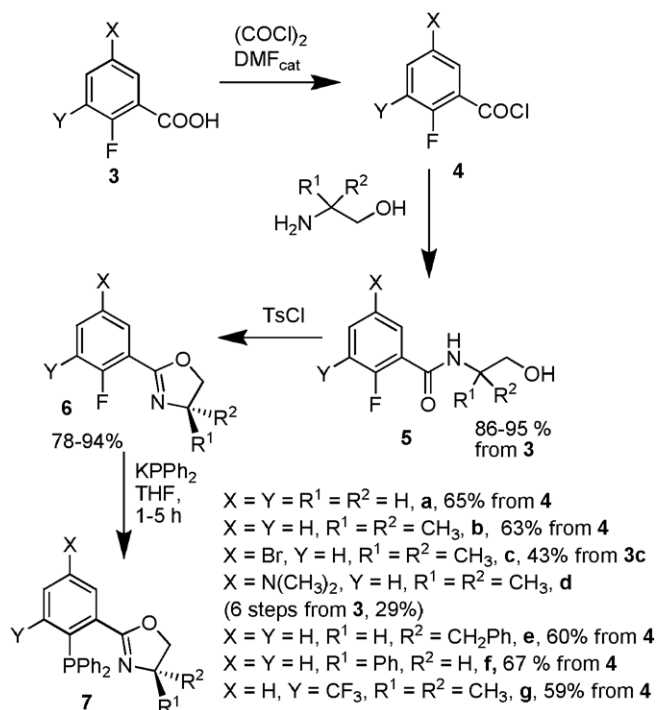
Scheme 1. Synthesis of sterically and electronically tuned PHOX ligands and overall yields.
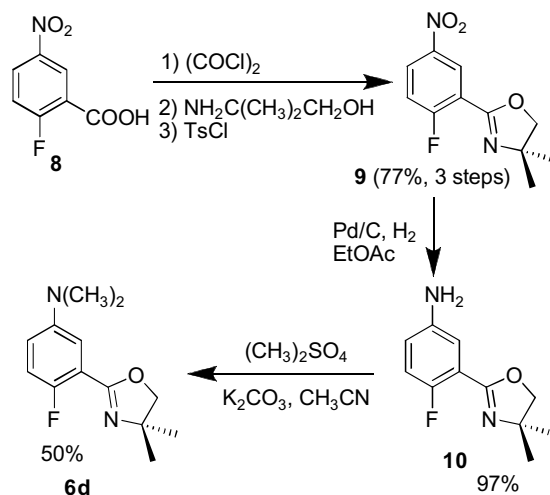
Scheme 2. Synthesis of an amine-containing oxazoline.

(1)
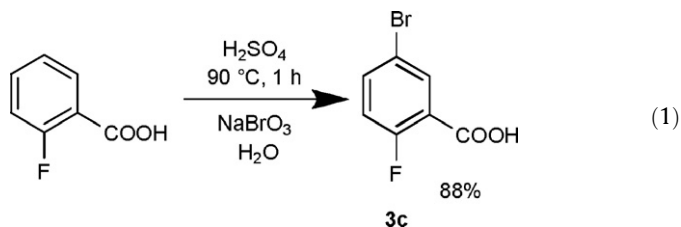
To place an electron-donating group on the phenyl ring, the dimethyl amino PHOX ligand 7d was synthesized as shown in Scheme 2 for 6d followed by conversion of 6d to 7d as shown in Scheme 1. Commercial 2-fluoro-5-nitrobenzoic acid (8) first was converted to the corresponding oxazoline 9 employing the three step standard procedure described above (Scheme 2). Subse-

quently, the nitro group in **9** was reduced to the amine with Pd/C and H_2 to obtain the amine **10** in 97% yield. The amine was then doubly methylated using dimethyl sulfate ((CH_3)$_2$$SO_4$) affording the dimethyl amino oxazoline **6d** in 50% yield. The methylation is needed, as the amino substituent in **10** is not compatible with the basic $KPPh_2$ used in the last step to introduce the PPh_2 group. The new PHOX ligand **7d** was obtained in 23% overall yield from **8** (6 steps, Schemes 1 and 2).
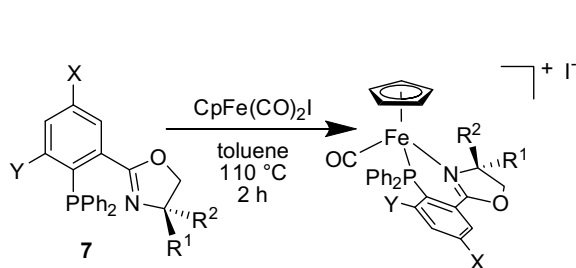
To place an electron withdrawing group on the ring system, commercial 2-fluoro-3-(trifluoromethyl)benzoyl chloride (**4g**) was subjected to the standard reaction sequence shown in Scheme 1. The new PHOX ligand **7g** features a CF_3 substituent in position ortho to the PPh_2 group and was obtained in 59% overall yield from **4g**.

Experimental details and spectroscopic data (including ^{19}F NMR) for all precursors are given in the Supplementary material. The final phosphorylation step with $KPPh_2$ leading to the new PHOX ligands **7c**, **7d**, and **7g** is described in Section 5. The new ligands were obtained as oils, some of which solidified over the course of several weeks and were characterized by NMR (^{1}H, ^{13}C, ^{31}P), mass spectrometry, IR and microanalysis. The substitution pattern on the oxazoline and on the phenyl ring has some impact on the chemical shift of the phosphorus atom in the ^{31}P NMR. Typically, the PHOX ligands described herein give signals between −4.0 and −4.8 ppm. The PHOX ligand **7d** bearing the electron-donating NMe_2 group, however, has a ^{31}P NMR chemical shift of −6.8 ppm and ligand **7g** featuring an electron withdrawing CF_3 group has a shift of 0.6 ppm.

2.2. Synthesis of new iron phosphinooxazoline complexes

For incorporation of a PHOX ligand into an iron complex, the cyclopentadienyl complex $CpFe(CO)_2I$ was selected as a precursor as it is readily available by iodination of commercial iron carbonyl dimer [$CpFe(CO_2)$]$_2$ [19]. The complex $CpFe(CO)_2I$ is known to give iodide salts of the half-sandwich complexes of the type [$CpFe(CO)_2(L)$]$^+$ when treated with monodentate donor ligands [20]. Reactions with bidentate ligands to give the iodide salts of the half-sandwich complexes [$CpFe(CO)(L–L)$]$^+$ are less common but a few examples have been described in the literature [21]. We anticipated that the CO ligand would be a sensitive probe for the electron density at the iron center, which typically impacts the carbonyl stretching frequency in the IR spectrum.

Accordingly, the PHOX ligands **7a–d** were reacted with $CpFe(CO)_2I$ (toluene, 110 °C, 2 h) form which the desired product precipitated. Recrystallization from CH_2Cl_2/Et_2O provided the new target compounds [**11a–d**]$^+$[I]$^-$ as red powders in 87–21% yields which will subsequently be referred to without charges (Scheme 3).
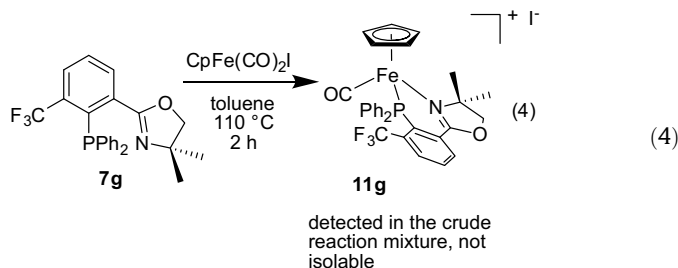
The new iron complexes are all chiral at the metal. Accordingly, the achiral PHOX ligands **7a–d** gave racemic mixtures of the corresponding metal complexes [**11a–d**][I]. However, chiral PHOX ligands would afford two separable diastereomeric isomers when employed in the metal complex synthesis shown in Scheme 3. Thus, (*S*)-**7e** was reacted with $CpFe(CO)_2I$ under the standard conditions described (Eq. (2)). A 1:1 mixture of the two diastereomeric complexes [**11e**][I] and [**11e′**][I] formed, as assessed by ^{31}P NMR of the crude reaction mixture. Efforts to separate the stereoisomers and to obtain diastereomerically pure material have failed so far.

(2)

76% (**11e** + **11e′**)
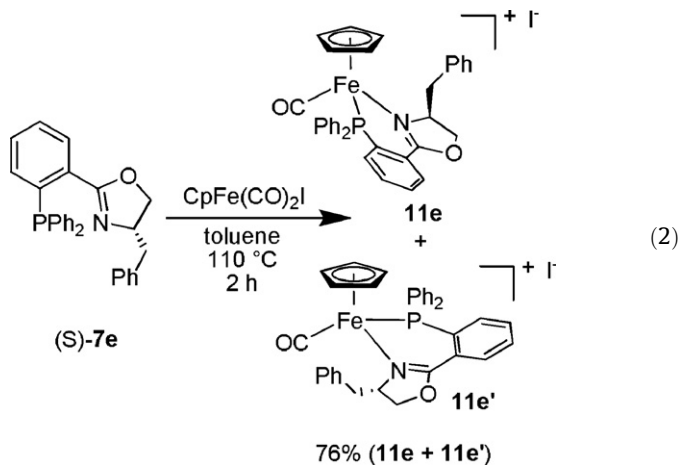
However, the PHOX ligand (*R*)-**7f** gave a 85:15 mixture of two diastereomers (^{31}P NMR) when reacted with $CpFe((CO)_2I$ (Eq. (3)), and it was possible to isolate the major diastereomer [**11f**][I] by fractional crystallization in 63% yield.

(3)

one diastereomer
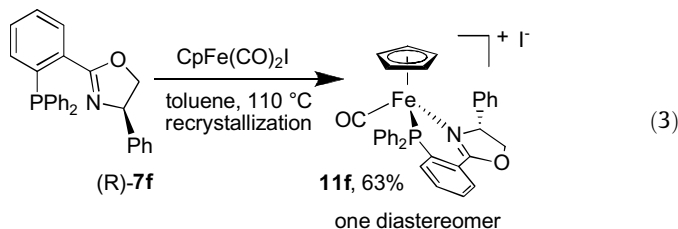
Finally, we attempted conversion of the PHOX ligand **7g** (featuring a CF_3 substituent in position ortho to the PPh_2) to the corresponding iron complex (Eq. (4)). After employing the standard procedure described, complex [**11g**] could be detected in the crude reaction mixture by mass spectrometry, IR and ^{31}P NMR. However, all efforts to isolate the PHOX iron complex [**11g**][I] have failed to date (as a result of continuing decomposition during attempts to separate the desired product).

Scheme 3. Synthesis of iron PHOX complexes [**11a–d**][I].

X = Y = R^1 = R^2 = H, **11a**, 66%
X = Y = H, R^1 = R^2 = CH_3, **11b**, 47%
X = Br, Y = H, R^1 = R^2 = CH_3, **11c**, 87%
X = NMe_2, Y = H, R^1 = R^2 = CH_3, **11d**, 21%

(4)

11g

detected in the crude reaction mixture, not isolable

We assume an intrinsic instability of complex [**11g**][I], because the crude reaction mixture contained a major side product, as seen by a peak in the ^{31}P NMR at −57.3 ppm, which did not disappear after purification attempts. Presumably the iodide counter ion undertakes (aided by the electron withdrawing CF_3 group) a nucleophilic attack on the central aromatic ring, displacing the PPh_2 group.

All new iron PHOX complexes [11a–d][I] and [11f][I] were characterized by NMR (^{1}H, ^{13}C, ^{31}P), mass spectrometry, IR, and microanalysis. All iron complexes except for [11f][I] were isolated as CH_2Cl_2 solvates, as seen in the microanalyses and the ^{1}H and ^{13}C NMR spectra. The solvent could not completely be removed *in vacuo*, even at elevated temperatures. Accordingly, all X-ray structures (*vide infra*) except for that of [11f][I] exhibited solvent molecules in the crystal lattice.

The coordination of the PHOX ligand was best seen by the large downfield shift of the phosphorus signal in the ^{31}P NMR spectrum. The free ligands have chemical shifts of around −4.5 ppm, whereas the iron complexes exhibited signals between 61.3 and 67.0 ppm. Due to coordination of the PHOX ligand to the iron center, the two phenyl rings on phosphorus become diastereotopic, and give in principle different ^{13}C NMR signals for each carbon atom (but the peaks are in practice not always resolved). Some of the aromatic carbon atoms couple with the phosphorus (J_{CP} = 2–11 Hz). As a consequence, a complex ^{13}C NMR spectrum in the aromatic region was observed. However, the number of signals did not reach the number of diastereomeric aromatic carbons, and some of the peaks had shoulders (or other non-Gaussian features).

The CO ligand was observed in the IR spectra, in the ^{13}C NMR and in the mass spectra. All new complexes showed one $\nu_{C\equiv O}$ stretching frequency in the IR spectrum; they are listed in Table 1 and show some dependency on the ligand structure (*vide infra*). In the ^{13}C NMR spectra, the CO carbon gave a doublet between 216.9 and 219.2 ppm (J_{CP} = 27.7–29.8 Hz), which is in accordance with related cyclopentadienyl iron carbonyl complexes [20a]. The FAB mass spectra showed a strong peak for the cationic portion of the metal complex, and an equally strong peak arising from loss of CO.

Finally, the geminal protons in all complexes [11a–f] and the geminal methyl groups of the oxazoline rings in [11b–c] are diastereotopic, and consequently give separate signals in the ^{1}H and ^{13}C NMR, respectively.

Complex [11f] is both chiral at the metal and at the ligand, and potentially two diastereomers form upon synthesis, which are distinguishable by NMR. Accordingly, two signals were observed in the ^{31}P NMR spectra of the crude reaction mixture and also two signals for the Cp ring in the ^{13}C NMR. Also, some resonances in the ^{1}H NMR were doubled. After fractional recrystallization, [11f] was obtained as single diastereomer, as best seen in the NMR spectra. In the ^{31}P NMR, only one signal was observed. The three H atoms on the oxazoline ring in [11f] are diastereotopic. They gave three signals in the ^{1}H NMR spectrum, as expected for a diastereopure compound. In the ^{13}C NMR, only one signal for the Cp ligand was observed.

All metal complexes were obtained as orange-red powders. They are poorly soluble in hexanes, $CHCl_3$ and diethyl ether, but well soluble in CH_2Cl_2, methanol and acetone. The metal complexes slowly decompose in CH_2Cl_2 solutions. The decomposition involves oxidation to paramagnetic iron(III) species, as seen by line broadening of corresponding aged NMR samples.

2.3. Further analysis of the phosphinooxazoline iron complexes

2.3.1. X-ray structure analyses

To unequivocally establish the structures of the new iron PHOX complexes, the crystal structure of selected iodide complexes was determined (Table 2 and Section 5). Complexes [11a][I], [11c][I], and [11d][I] crystallized readily, but the other complexes did not give crystals of X-ray quality. To obtain material that crystallized more easily, the iodide counter ion in [11b][I] was exchanged by ClO_4^- to give [11b][ClO$_4$] and in [11f][I] by PF_6^- to give [11f][PF$_6$] as described in Section 5.

The molecular structures are depicted in Figs. 2 and 3 and Table 3 lists key structural data.

The bond angles around iron range from 83.2(3)° for the N(1)–Fe(1)–P(1) angle to 100.00(8)° for the C(1)–Fe–P(1) angle. Thus, the coordination geometry of the complexes is best described as a slightly distorted octahedron. The deviations for the C(1)–Fe–N(1) angles from ideal 90° are the largest for complexes [11b], [11c] and [11d] (99.2(6)–100.00(8)°, see entry 9 in Table 3). These complexes bear two methyl substituents in the position α to the nitrogen in the oxazoline ring. Complex [11a] bears two hydrogen atoms in this position and [11f] one phenyl ring, and their C(1)–Fe–N(1) angle is closer to the ideal 90°. Obviously the two methyl groups in [11b], [11c] and [11d] increase – due to steric interactions – the C(1)–Fe–N(1) angle. In turn, the deviation from linearity for the CO ligand are the greatest for [11b], [11c] and [11d] (174.64(19)–170.7(16)°, entry 12 in Table 3), presumably due to the same steric interaction with the two methyl groups.

The structural differences between [11a] and [11f] on the one hand and [11b], [11c] and [11d] on the other hand are best seen in the overlay of the structures of [11a] and [11b] shown in Fig. 4. In complex [11a], the oxazoline ring plane is oriented almost parallel to the axis formed by the iron and the Cp centroid; the phenyl ring attached to the oxazoline points away from the Cp. In [11b], the oxazoline plane is oriented perpendicular to this axis, and the phenyl ring points towards the Cp ring.

The Fe–C bond distances between the iron center and the carbon atoms of the cyclopentadienyl ring are not all equal (Table 3, entries 5–7). The Fe–C bond distances trans to the phosphorus and the CO ligand are slightly longer than the bond distances trans to the nitrogen. This effect has been previously described and might be associated with the stronger trans influence of phosphorus and CO ligands [10a,b].

The bite angles N(1)–Fe–P(1) (Table 3, entry 10) of the phosphinooxazoline ligand vary by only a small amount with the substituent, being the biggest for the oxazoline with a phenyl substituent α to nitrogen in [11f] (86.92(9)°), and the smallest in [11d] (83.2(3)°) having two methyl substituents in that position.

Due to coordination of the PHOX ligand to the iron center, a six-membered chelate ring forms, containing the atoms Fe–N(1)–C(9)–(C10)–(C15)–P(1). This chelate ring is best described as an envelope conformer and is here analyzed as previously described by Helmchen and co-workers [22]. All calculations were performed using MERCURY 1.4.2 software.

As shown in Fig. 5, five of the six ring atoms – N(1)–C(9)–(C10)–(C15)–P(1) – nearly form a plane. The involved atoms deviate from the ideal plane by an average value given in Table 4 and the largest deviation from planarity was observed for complex [11a] (0.165 Å). The iron center is located above this plane. The ideal N(1)–C(9)–(C10)–(C15)–P(1) plane and the plane spanned by the iron center and the two coordinated N(1) and P(1) atoms form an angle α

Table 1
Physical data of iron PHOX complexes

Complex	$\nu_{C\equiv O}$ (cm^{-1})	C≡O bond distance (Å)	$E_{1/2}^c$ (V)	ΔE^c (V)	i_c/i_a^c	E_{pa}^c (V)	E_{pa}^d (V) Free ligand 7
[11a][I]	1971	1.138(3)	1.00	0.43	0.90	1.21	0.92
[11b][I]	1944	1.150(3)^a	1.28	0.36	1.0	1.46	0.86
[11c][I]	1947	1.159(13)	1.20	0.24	0.95	1.32	1.13
[11d][I]	1951	1.16(2)	1.01	0.33	1.0	1.18	0.87
[11e][I]	1950						1.09
[11f][I]	1967	1.142(3)^b	1.00	0.35	0.95	1.18	0.82

^{a} [11b][ClO$_4$].
^{b} [11f][PF$_6$].
^{c} Data from cyclic voltammetry experiments for the first redox couple, referenced against ferrocene as internal standard (see Section 5). All complexes with [PF$_6$]$^-$ counter ions.
^{d} First oxidation potential.

Table 2
Crystallographic parameters

	[11a][I] · (CH₂Cl₂)	[11b][ClO₄] · (CH₃COCH₃)	[11c][I] · (CH₂Cl₂) · (I₂)₀.₅	[11d][I] · (CHCl₃)₄ · (Et₂O)(H₂O)	[11f][PF₆]
Empirical formula	$C_{28}H_{25}Cl_2FeINO_2P$	$C_{32}H_{33}ClFeNO_7P$	$C_{60}H_{56}Br_2Cl_4Fe_2I_3N_2O_4P_2$	$C_{70}H_{82}Cl_{12}Fe_2I_2N_4O_7P_2$	$C_{33}H_{27}F_6FeNO_2P_2$
Formula weight	692.11	665.86	1725.03	1944.24	701.35
Temperature (K)/ wavelength (Å)	566(2)/0.71073	100(2)/0.71073	100(2)/0.71073	100(2)/0.71073	100(2)/0.71073
Crystal system	Monoclinic	Monoclinic	Triclinic	Monoclinic	Monoclinic
Space group	$P2_1/c$	$P2_1/c$	$P\bar{1}$	$P2_1/c$	$P2_1$
Unit cell dimensions					
a (Å)	14.0012(4)	13.7233(9)	13.4019(13)	23.558(2)	9.3227(6)
b (Å)	19.8125(6)	13.1971(9)	14.9871(17)	13.0156(12)	16.4376(11)
c (Å)	11.1039(3)	17.6282(12)	17.2908(19)	26.819(2)	9.8896(7)
α (°)	90	90	112.900(6)	90	90
β (°)	112.9750(10)	110.192(4)	95.131(6)	97.192(4)	96.765(3)
γ (°)	90°	90	90.428(6)	90	90
Volume (Å³)/Z	2835.87(14)/4	2996.4(3)/4	3183.0(6)/2	8158.8(12)/4	1504.96(18)/2
D_{calc} (Mg/m³)	1.621	1.476	1.800	1.583	1.548
Absorption coefficient (mm⁻¹)	1.891	0.696	3.430	1.596	0.678
$F(000)$	1376	1384	1682	3912	716
Crystal size (mm)	0.35 × 0.28 × 0.26	0.26 × 0.13 × 0.12	0.24 × 0.07 × 0.06	0.33 × 0.20 × 0.18	0.27 × 0.20 × 0.11
θ Range for data collection (°)	2.87–27.15	2.78–26.47	1.53–25.00	1.66–25.00	3.10–26.44
Index ranges	−17 ⩽ h ⩽ 17, −24 ⩽ k ⩽ 25, −13 ⩽ l ⩽ 14	−17 ⩽ h ⩽ 17, −16 ⩽ k ⩽ 16, −22 ⩽ l ⩽ 22	−15 ⩽ h ⩽ 15, −17 ⩽ k ⩽ 17, −20 ⩽ l ⩽ 20	−27 ⩽ h ⩽ 25, −15 ⩽ k ⩽ 14, −31 ⩽ l ⩽ 31	−11 ⩽ h ⩽ 11, −20 ⩽ k ⩽ 20, −12 ⩽ l ⩽ 12
Reflections collected	69770	73411	85151	75358	32208
Independent reflections (R_{int})	6262 (0.037)	6095 (0.068)	11119 (0.196)	14254 (0.12)	6138 (0.058)
Completeness to θ = 27.15° (%)	99.7	98.2	99.2	99.2	99.2
Absorption correction	Numerical	Numerical	Semi-empirical from equivalents	Numerical	Numerical
Maximum and minimum transmission	0.6877 and 0.6279	0.9211 and 0.8398	0.8206 and 0.4932	0.8382 and 0.7366	0.9280 and 0.8376
Refinement method	Full-matrix least-squares on F^2	Full-matrix least-squares on F^2	Full-matrix least-squares on F^2	Full-matrix least-squares on F^2	Full-matrix least-squares on F^2
Data/restraints/ parameters	6262/6/343	6095/0/392	11119/0/658	14254/9/865	6138/55/454
Goodness-of-fit on F^2	1.032	1.035	0.991	1.810	1.050
Final R indices [$I > 2\sigma(I)$]	$R_1 = 0.0337, wR_2 = 0.0796$	$R_1 = 0.0347, wR_2 = 0.0739$	$R_1 = 0.0728, wR_2 = 0.1534$	$R_1 = 0.1304, wR_2 = 0.2835$	$R_1 = 0.0387, wR_2 = 0.0732$
R indices (all data)	$R_1 = 0.0522, wR_2 = 0.0887$	$R_1 = 0.0500, wR_2 = 0.0795$	$R_1 = 0.1546, wR_2 = 0.1870$	$R_1 = 0.1948, wR_2 = 0.2988$	$R_1 = 0.0512, wR_2 = 0.0776$
Largest difference in peak and hole (e Å⁻³)	0.463 and −0.394	0.420 and −0.364	1.964 and −1.736	5.216 and −2.146	0.346 and −0.311
Absolute structure parameter					−0.015(13)

(Fig. 5). The angle α depends on the PHOX ligand (Table 4), being the greatest for [**11b**], [**11c**], and [**11d**] (52.35–55.32°, with two methyl substituents on the oxazoline ring), somewhat smaller for [**11a**] (42.66°, no substituent on the oxazoline ring) and the smallest for [**11f**] (41.02°, one phenyl on the oxazoline ring). The two phenyl groups on phosphorus occupy pseudoaxial and pseudoequatorial positions and are thus diastereotopic.

The angle between the best fit planes of the oxazoline ring and the phenyl ring, to which it is connected, was also calculated (Table 4). The angle is the smallest for [**11a**] and [**11f**] (13.19–14.99°) and larger for the oxazoline ring bearing two methyl groups in [**11b**], [**11c**] and [**11d**] (21.95–27.96°). Finally, the distance between the iron center and the centroid of the cyclopentadienyl ring was calculated (Table 4). These values only range between 1.714 and 1.729 Å and depend very little on the ligand structure.

Complex [**11f**] is chiral at the metal. According to the priority order C₅H₅ > P > N > C [10,23], the absolute configuration of this complex is (R), as determined from the X-ray structure. However, a racemic crystal of [**11f**] was also found in the crystallized material. Attempts were made to determine the optical purity of the bulk sample, but solutions of [**11f**] are intensely colored, making the determination of optical rotations difficult, even at different wavelengths [24]. NMR experiments with chiral shift reagents

did not give meaningful results. However, the optical rotation of the ligand **7f** employed in metal complex synthesis was close to the literature value [18]. The enantiomer of [**11f**] required a change of the absolute configuration at the ligand. We are not aware of a mechanism that could largely racemize the ligand. Thus, we assume [**11f**] is of high optical purity.

2.3.2. Cyclic voltammetry

In order to obtain preliminary insight into the electronic properties of the new metal complexes, cyclic voltammograms of the PHOX ligands and the iron PHOX complexes were recorded as described in Section 5. Key data are listed in Table 1 and the traces are given in the Supplementary material.

The cyclic voltammograms of the ligands suggest complex and irreversible chemical reactions taking place [25]. Scans towards increasing positive potential show a varying number of irreversible oxidation waves without reduction waves on the reverse scan. No signs of greater reversibility were observed at higher scan rates up to 2 V s⁻¹ and faster scans further impeded the electron transfer. The potentials of the free PHOX ligands for the first oxidation differed between 0.82 and 1.13 V. The oxidation potentials show a slight dependency on the substituents. For example, ligand **7b** has an oxidation potential E_a of 0.86 V, whereas ligand **7c** – bearing
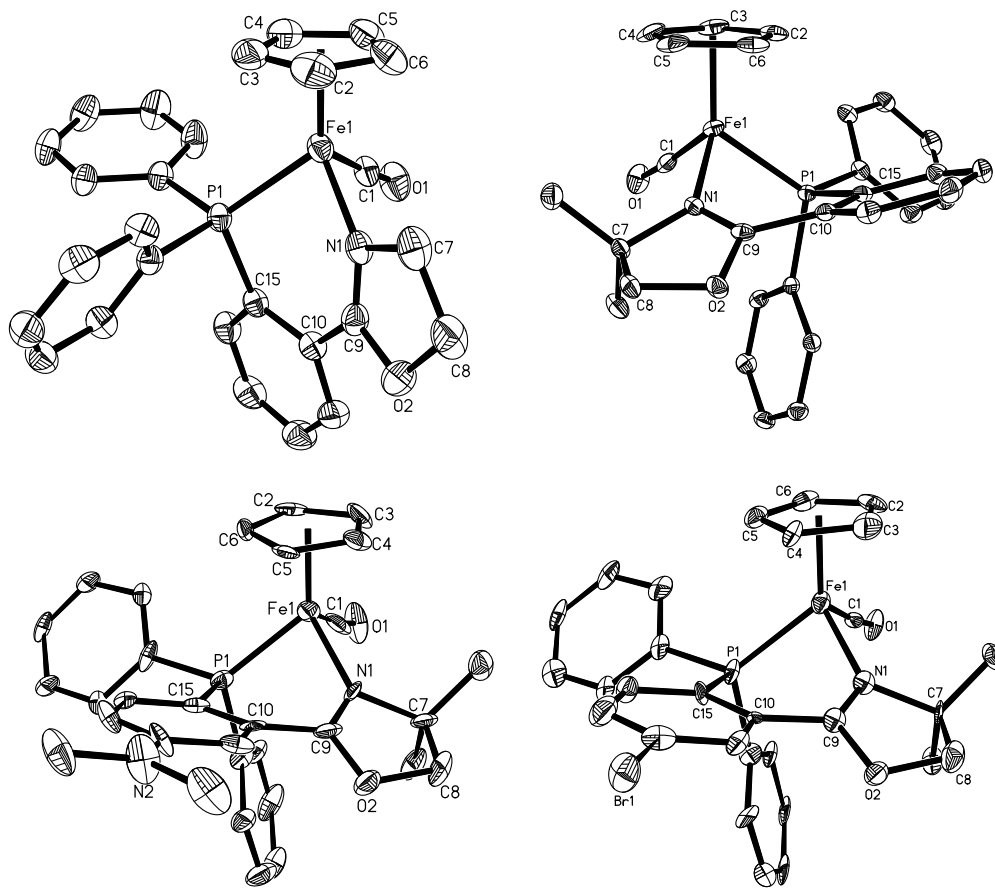
Fig. 2. Molecular structures of iron PHOX complexes [**11a**][I], [**11b**][ClO₄] (top) and [**11c**][I], [**11d**][I] (bottom). Counter ions and solvent molecules are omitted for clarity.
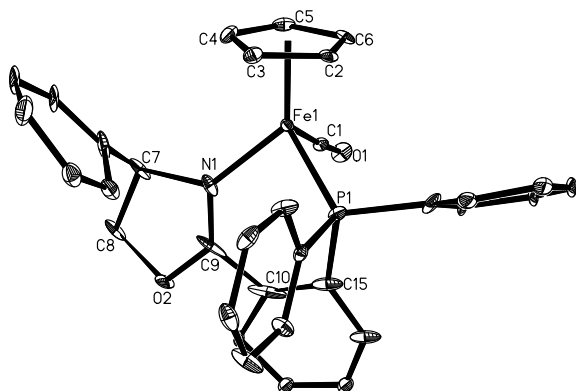

Fig. 3. Molecular structures of iron PHOX complex [**11f**][PF₆]. Counter ion omitted for clarity.

a bromo substituent – has an oxidation potential of 1.13 V. As expected, the electron withdrawing bromo substituent increases the oxidation potential of the PHOX ligand.

The cyclic voltammograms for the corresponding metal complexes show a fair degree of reversibility in that a reduction wave is seen for each complex that appears similar in size and is of complimentary shape to the first oxidation wave. The $E_{1/2}$ values for the first oxidation range from 1.00 to 1.28 V and the peak current ratios i_c/i_a are $\geqslant 0.9$. While the ideal separation between the oxidation and reduction peaks for a diffusing species undergoing a one-electron oxidation–reduction cycle is 59 mV, the peak-to-peak separations ΔE seen here are between 0.24 and 0.43 V suggesting

sluggish electron transfer. At higher potentials, additional irreversible oxidation waves were observed for almost all complexes. The complex electrochemical reactions taking place at higher oxidation states remain as a subject of future study.

Whereas the ligands alone show irreversible electrochemical behavior, the formation of the complex yields much greater signs of reversibility. This suggests that a one-electron oxidation and reduction is occurring that involves a highest occupied molecular orbital found only for the complex and not for the ligand alone. The relationship between E_a and the $\nu_{C=O}$ stretching frequency will be discussed in the next section.

3. Discussion

This study shows for the first time the isolation and characterization of a series of stable PHOX chelate complexes of iron. Steric and electronic properties are influenced by the structure of the PHOX ligand.

The steric properties of the new the iron complexes described above are basically governed by the substituents α to the nitrogen atom on the oxazoline ring as shown by the crystallographic data. Complex [**11a**] bearing no substituent α to the nitrogen in the oxazoline ring system crystallographically resembles [**11f**], bearing one phenyl substituent in that position. Complexes [**11b**], [**11c**] and [**11c**] bear two methyl groups in this position and are structurally related as well. The geminal methyl groups cause changes in the structure of the corresponding complexes, as shown in Fig. 4.

The properties of the new iron complexes were further analyzed by means of X-ray structure analysis, oxidation potentials determined by cyclic voltammetry and by evaluation of the IR spectra

Table 3
Selected bond lengths, angles and torsion angles for iron PHOX complexes

Entry	Complex	[11a][I]	[11b][ClO₄]	[11c][I]	[11d][I]	[11f][PF₆]
Bond lengths (Å)						
1	Fe–C(1)	1.753(3)	1.754(2)	1.755(13)	1.75(3)	1.763(3)
2	Fe–N(1)	1.980(2)	1.9788(17)	1.989(9)	1.983(11)	1.988(3)
3	Fe–P(1)	2.1891(7)	2.1950(6)	2.192(4)	2.197(4)	2.1868(9)
4	N(1)–C(9)	1.274(4)	1.285(2)	1.271(14)	1.277(18)	1.292(5)
5	Fe–C(X) (trans to CO)	2.110(3)[a]	2.100(2)[b]	2.103(12)[c]	2.082(16)[d]	2.122(3)[e]
6	Fe–C(Y) (trans to N)	2.088(3)[a]	2.080(2)[b]	2.068(11)[c]	2.078(13)[d]	2.079(3)[e]
7	Fe–C(Z) (trans to P)	2.103(3)[a]	2.112(2)[b]	2.137(12)[c]	2.111(14)[d]	2.096(3)[e]
8	C(1)–O(1)	1.138(3)	1.150(3)	1.159(13)	1.16(2)	1.142(3)
Bond angles (°)						
9	C(1)–Fe–N(1)	92.62(12)	100.00(8)	99.4(4)	99.2(6)	91.57(14)
10	N(1)–Fe–P(1)	85.23(7)	83.38(5)	84.2(3)	83.2(3)	86.92(9)
11	C(1)–Fe–P(1)	92.32(9)	93.58(7)	96.2(4)	96.5(5)	92.90(11)
12	O(1)–C(1)–Fe	176.6(3)	174.64(19)	173.6(10)	170.7(16)	176.2(3)
Torsion angles (°)						
13	N(1)–C(9)–C(10)–C(15)	−17.8(4)	−31.8(3)	25.1(18)	33(2)	20.1(6)

[a] $X = 2$, $Y = 4$, $Z = 6$.
[b] $X = 6$, $Y = 3$, $Z = 4$.
[c] $X = 4$, $Y = 6$, $Z = 2$.
[d] $X = 5$, $Y = 2$, $Z = 3$.
[e] $X = 3$, $Y = 6$, $Z = 5$.
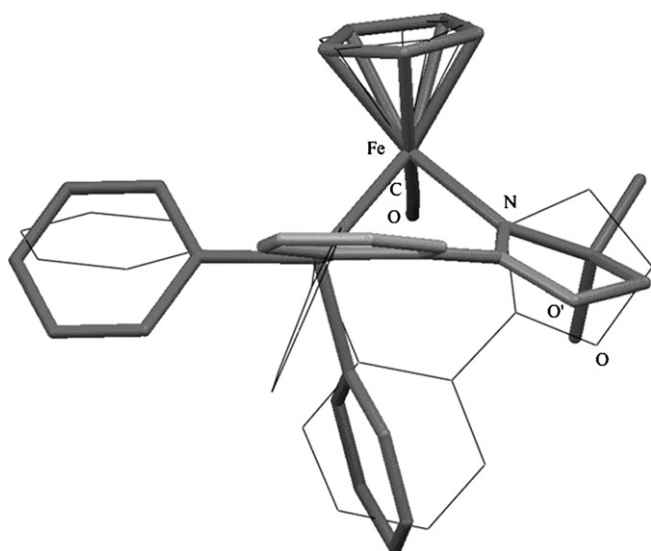
Fig. 4. Overlay of the molecular structures of [11a][I] (thin lines) and [11b][ClO₄] (thick lines). For the overlay, the inverted structure of [11b][ClO₄] was used.
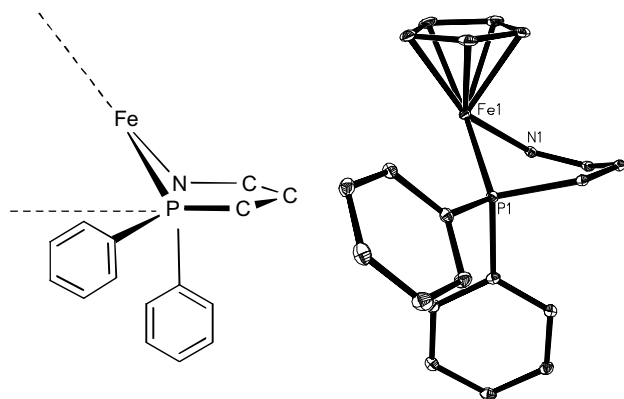
Fig. 5. Geometry of the six-membered metallacycle formed upon coordination and a corresponding part of the molecular structure of [11b] (whose inverted structure was used for this representation).

Table 4
Structural parameters calculated from X-ray data

Complex	[11a]	[11b]	[11c]	[11d]	[11f]
Envelope angle α[a] (°)	42.66	55.32	52.35	53.91	41.02
Deviation from planarity[b] (Å)	0.165	0.116	0.107	0.107	0.087
Oxazoline–Ph angle[c] (°)	14.99	27.96	21.95	24.86	13.19
Fe–Cp distance[d] (Å)	1.729	1.725	1.714	1.723	1.723

[a] The angle between an idealized plane formed by N(1)–C(9)–C(10)–C(15)–P(1) and the N(1)–Fe–P(1) plane, see Fig. 5.
[b] Average distance of the involved atoms from the ideal N(1)–C(9)–C(10)–C(15)–P(1) plane.
[c] The angle between an idealized plane formed by the oxazoline ring and the plane of the phenyl to which it is attached.
[d] Distance between the Cp centroid and Fe.

(Table 1). In general, strongly electron-donating ligands increase the electron density at the metal center. As a consequence, the oxidation potential of the metal complex should decrease. In addition, electron rich metal centers increase back bonding into the π* orbitals of the carbonyl ligand. This weakens the C≡O bond, resulting in increased bond lengths and lowered IR $\nu_{C≡O}$ stretching frequencies.

Some dependency of the ligand structure on the oxidation potential of the corresponding iron complex was observed. For most of the cases, the oxidation potentials of the iron complexes do not follow a clear trend (Table 1). For example, complex [11d] with the PHOX ligand bearing an electron-donating dimethyl amino group has about the same oxidation potential (1.01 V) as complex [11f] without the dimethyl amino group but with one phenyl substituent α to the oxazoline nitrogen (1.00 V). Strictly speaking, the E_a values for the free ligands and the $E_{1/2}$ values for the metal complexes cannot be compared. However, the potentials of the ligands seem to be generally similar to those of their respective metal complexes, suggesting a ligand-centered HOMO.

The $\nu_{C≡O}$ stretching frequencies, which range from 1944 to 1971 cm⁻¹, vary only little with the PHOX ligand. Complex [11a], which bears substituents neither on the phenyl core nor on the oxazoline ring, shows the highest stretching frequency of 1971 cm⁻¹. Complex [11f] ($\nu_{C≡O}$ = 1967 cm⁻¹), bearing one phenyl ring α to the oxazoline nitrogen, closely resembles complex [11a]. For all other complexes, the ligand has only a small influence on

the IR stretching frequencies, which range from 1944 to 1951 cm^{-1}. If at all, it seems that the substituent α to the nitrogen in the oxazoline ring has the biggest influence on the $v_{C\equiv O}$ stretching frequencies.

Similarly, the CO bond distances for the structurally characterized metal complexes range from 1.138(3) to 1.159(13) and show only little dependency on the ligand structure.

The relationship between $E°$ and $v_{C\equiv O}$ has been discussed by Eriks and Giering [26]. They established a linear dependency of the stretching frequency $v_{C\equiv O}$ on the reduction potential $E°$ for structurally related iron carbonyl complexes bearing a purely σ-donating phosphine ligand. But ligands with both σ-donor/π-acceptor capability exhibited considerable scatter of linearity in this study. The PHOX ligands described herein feature in the oxazoline ring a sp^2 hybridized nitrogen atom capable of backbonding. Furthermore, the electrochemical data point towards a ligand-centered HOMO, whereas the $v_{C\equiv O}$ reflects the electron density at the metal. These might be the reasons why a linear dependency of the electron density of the ligand and the oxidation potential of its corresponding metal complex could not be observed.

Furthermore, analysis and comparison of trends described above are, strictly speaking, possible only for structurally related complexes. The X-ray analysis data show that the complexes differ somewhat in their geometry (see e.g. Fig. 4 or the Fe–C(1)–(O) angles which show noticeable deviation from linearity, as seen in entry 12 in Table 2), which also might explain deviations from idealized trends.

4. Conclusion

In conclusion, we have for the first time synthesized a series of chelating PHOX complexes of iron, which were structurally and spectroscopically analyzed. The crystallographically determined bond lengths of the CO ligand and its $v_{C\equiv O}$ stretching frequencies vary only slightly with the ligand, but some dependence of the oxidation potential of the complexes on the ligand structure was observed. The novel PHOX complexes established herein potentially allow for applications of iron catalysts in organic syntheses and such studies are currently underway.

5. Experimental

5.1. General methods

Chemicals were treated as follows: THF, toluene, diethyl ether, distilled from Na/benzophenone; CH$_2$Cl$_2$, distilled from CaH$_2$; KPPh$_2$, (Aldrich, 0.5 M in THF), NaPF$_6$ (Aldrich) used as received. The syntheses of 2-(5-bromo-2-fluorophenyl)-4, 4-dimethyl-4,5-dihydro-1,3-oxazole (**6c**), 3-(4,4-dimethyl-4,5-dihydro-1,3-oxazol-2-yl)-4-fluoro-*N,N*-dimethylaniline (**6d**), and 2-[2-fluoro-3-(trifluoromethyl)phenyl]-4,4-dimethyl-4,5-dihydro-1,3-oxazole (**6g**) and intermediates (if required) are described in the Supplementary material. CpFe(CO)$_2$I was synthesized according to the literature [19].

NMR spectra were obtained at room temperature on a Bruker Avance 300 MHz or a Varian Unity Plus 300 MHz instrument and referenced to a residual solvent signal; all assignments are tentative. GC/MS spectra were recorded on a Hewlett Packard GC/MS System Model 5988A. Exact masses were obtained on a JEOL MStation [JMS-700] Mass Spectrometer. Melting points are uncorrected and were taken on an Electrothermal 9100 instrument. IR spectra were recorded on a Thermo Nicolet 360 FT-IR spectrometer. UV–Vis spectra were recorded on a Varian Cary 100 UV–Vis spectrophotometer. Elemental analyses were performed by Atlantic Microlab Inc., Norcross, GA, USA.

5.2. Synthesis of the ligands

5.2.1. Synthesis of 2-[5-bromo-2-(diphenylphosphino)phenyl]-4,4-dimethyl-4,5-dihydro-1,3-oxazole (*7c*)

A Schlenk flask was charged with the aryl fluoride **6c** (0.552 g, 2.029 mmol) and KPPh$_2$ (0.5 M in THF, 4.5 mL, 2.3 mmol) was added dropwisely with stirring. The resulting reddish solution was refluxed for 1 h. The reaction mixture was diluted with CH$_2$Cl$_2$ (50 mL) and poured into a saturated aqueous solution of NaHCO$_3$ (25 mL). The organic layer was separated, washed with H$_2$O and dried over MgSO$_4$. The solution was concentrated in vacuo and the crude product purified by flash column chromatography on silica (1 × 15 cm column; eluted with 1:0 v/v toluene/EtOAc → 7:3 v/v toluene/EtOAc) to obtain the product (0.540 g, 1.23 mmol, 61%) as an oil which solidified over the course of several weeks to give a white solid. Anal. Calc. for C$_{23}$H$_{21}$BrNOP: C, 63.03; H, 4.83. Found: C, 62.75; H, 4.86%.

NMR (δ, CDCl$_3$) ^{1}H 8.02 (t, $^4J_{HH}$ = 2.6 Hz, 1H, H-6 aromatic), 7.38 (dd, $^3J_{HH}$ = 8.4, $^4J_{HH}$ = 2.2 Hz, 1H, H-4 aromatic), 7.29–7.34 (m, 10 H, P(C$_6$H$_5$)$_2$), 6.67 (dd, $^3J_{HH}$ = 8.3, $^3J_{HP}$ = 4.0 Hz, 1H, H-3 aromatic), 3.74 (s, 2H, CH$_2$O), 1.04 (s, 6H, 2CH$_3$); ^{13}C{^{1}H} 161.1 (d, $^3J_{CP}$ = 2.7 Hz, C=N), 138.0 (d, J_{CP} = 26. 9 Hz, Ph), 137.2 (d, J_{CP} = 11.0 Hz, Ph), 134.9 (d, J_{CP} = 2.7 Hz, Ph), 134.1 (d, J_{CP} = 21.4 Hz, Ph), 133.4 (d, J_{CP} = 18.1 Hz, Ph), 133.3 (s, Ph), 132.8 (d, J_{CP} = 2.2 Hz, Ph), 128.9 (s, Ph), 128.6 (d, J_{CP} = 7.7 Hz, Ph), 122.3 (d, J_{CP} = 1.1 Hz, Ph), 78.9 (s, CH$_2$O), 67.7 (s, C(CH$_3$)$_2$), 27.9 (s, 2CH$_3$); ^{31}P{^{1}H} – 4.7 (s).

MS (FAB, 3-NBA, *m/z*) [27] 476 ([**7c**+O+Na]$^+$, 100%), 454 ([**7c**+O]$^+$, 7%); IR (cm^{-1}, neat) $v_{C=N}$ 1643 (s).

5.2.2. Synthesis of 3-(4,4-dimethyl-4,5-dihydro-1,3-oxazol-2-yl)-4-(diphenylphosphino)-N,N-dimethylaniline (*7d*)

Aryl fluoride **6d** (0.122 g, 0.515 mmol) was converted as described above for **7c** to obtain **7d** (0.162 g, 0.403 mmol, 78%) as white crystals. Anal. Calc. for C$_{25}$H$_{27}$N$_2$OP: C, 74.61; H, 6.76. Found: C, 74.56; H, 6.75%.

NMR (δ, CDCl$_3$) ^{1}H 7.24–7.38 (m, 10H, P(C$_6$H$_5$)$_2$), 7.18 (t, $^4J_{HH}$ = 2.9 Hz, 1H, H-2 aromatic), 6.69 (dd, $^3J_{HH}$ = 8.7, $^3J_{HP}$ = 4.3 Hz, 1H, H-5 aromatic), 6.59 (dd, $^3J_{HH}$ = 8.7, $^4J_{HH}$ = 2.8 Hz, 1H, H-6 aromatic), 3.78 (s, 2H, CH$_2$O), 2.93 (s, 6H, N(CH$_3$)$_2$), 1.11 (s, 6H, 2CH$_3$); ^{13}C{^{1}H} 163.2 (d, $^3J_{CP}$ = 1.7 Hz, C=N), 149.9 (s, Ph), 139.0 (d, J_{CP} = 12.1 Hz), 134.7 (d, J_{CP} = 1.7 Hz, Ph), 133.8 (d, J_{CP} = 20.3 Hz, Ph), 133.4 (d, J_{CP} = 22.0 Hz, Ph), 128.2 (d, J_{CP} = 5.4 Hz, Ph), 128.1 (s, Ph), 122.6 (d, J_{CP} = 18.1 Hz, Ph), 114.0 (s, Ph), 113.5 (d, J_{CP} = 4.4 Hz, Ph), 78.7 (s, CH$_2$O), 67.5 (s, C(CH$_3$)$_2$), 40.1 (s, N(CH$_3$)$_2$), 28.0 (s, C(CH$_3$)$_2$); ^{31}P{^{1}H} – 6.8 (s).

MS (FAB, 3-NBA, *m/z*) [27] 425 ([**7d**+Na]$^+$, 68%), 441 ([**7c**+O+Na]$^+$, 48%); IR (cm^{-1}, neat) $v_{C=N}$ 1598 (s).

5.2.3. Synthesis of 2-[2-(diphenylphosphino)-3-(trifluoromethyl)phenyl]-4,4-dimethyl-4,5-dihydro-1,3-oxazole (*7g*)

Aryl fluoride **6g** (1.562 g, 5.98 mmol) was converted and worked up as described above for **7c** to obtain **7g** (2.07 g, 4.84 mmol, 81%) as slightly yellowish crystals. Anal. Calc. for C$_{24}$H$_{21}$F$_3$NOP: C, 67.44; H, 4.95. Found: C, 67.42; H, 5.02%.

NMR (δ, CDCl$_3$) ^{1}H 7.85–7.98 (m, 2 H, H-4, H-6 aromatic), 7.57 (t, $^3J_{HH}$ = 7.8 Hz, 1H, H-5 aromatic), 7.24–7.39 (m, 10H, 2C$_6$H$_5$), 3.46 (s, 2H, CH$_2$O), 1.01 (s, 6H, 2CH$_3$); ^{13}C{^{1}H} 163.1 (d, $^3J_{CP}$ = 2.2 Hz, C=N), 137.6 (d, J = 8.8 Hz, Ph), 137.6–136.1 (m, C-3 aromatic), 135.6 (s, Ph), 135.3 (dd, J = 13.5, 1.4 Hz, Ph), 135.2 (d, J = 41.7 Hz, Ph), 132.6 (d, J = 20.3 Hz, Ph), 129.5 (s, C-6 aromatic), 129.4–129.0 (m, Ph), 128.04 (d, J = 6.6 Hz, Ph), 128.03 (s, Ph), 123.8 (q, $^1J_{CF}$ = 275.5 Hz, CF$_3$), 78.3 (s, CH$_2$O), 67.1 (s, C(CH$_3$)$_2$), 27.8 (s, C(CH$_3$)$_2$); ^{31}P{^{1}H} 0.6 (q, $^4J_{PF}$ = 46.4 Hz); ^{19}F{^{1}H} – 55.7 (d, $^4J_{FP}$ = 46.4 Hz, CF$_3$).

MS (FAB, 3-NBA, *m/z*) [27] 466 ([**7g**+O+Na]$^+$, 100%), 450 ([**7c**+Na]$^+$, 19%); IR (cm^{-1}, neat) $v_{C=N}$ 1644 (s).

5.3. Synthesis of the iron complexes

5.3.1. Synthesis of "[CpFe(CO)(7a)][I] · (CH₂Cl₂)₀.₅", [11a][I] · (CH₂Cl₂)₀.₅

To a Schlenk flask containing PHOX **7a** (0.200 g, 0.604 mmol), CpFe(CO)₂I (0.166 g, 0.546 mmol) was added followed by toluene (2 mL) to obtain a dark suspension. The flask was immersed in an oil bath preheated to 110 °C, and the mixture was allowed to stir under nitrogen atmosphere at room temperature for 2.5 h. A red precipitate formed. The solvent was removed by high vacuum and the residue taken up in CH₂Cl₂ (2 mL) and filtered through a short pad of Celite® (rinsed with CH₂Cl₂). The red filtrate was concentrated to ca. 2 mL, layered with diethyl ether, and stored at −18 °C for 18 h. A red precipitate formed. The solvent was decanted, and the red residue dried under vacuum to obtain [**11a**][I] · (CH₂Cl₂)₀.₅ as a red solid (0.235 g, 0.361 mmol, 66%), m.p. 196–198 °C dec. (capillary). Anal. Calc. for $C_{27}H_{23}FeI$-$NO_2P \cdot (CH_2Cl_2)_{0.5}$: C, 50.84; H, 3.72. Found: C, 50.76; H, 3.79%.

NMR (δ, CD₂Cl₂) [28] ^1H 8.03–7.88 (m, 1H, Ph), 7.79–7.45 (m, 13H, Ph), 7.45–7.30 (s, 1H, Ph), 5.03–4.90 (s, 5H, Cp), 4.70–4.34 (m, 3H, CH₂ + CHH′), 4.01–3.84 (m, 1H, CHH′); $^{13}C\{^1H\}$ 167.5 (d, J_{CP} = 5.6 Hz, C=N), 133.6 (d, J_{CP} = 6.9 Hz, Ph), 133.1 (d, J_{CP} = 9.7 Hz, Ph), 132.6 (d, J_{CP} = 10.3 Hz, Ph), 132.3 (br, Ph), 132.1 (s, Ph), 131.8 (d, J_{CP} = 7.4 Hz, Ph), 131.6 (d, J_{CP} = 5.1 Hz, Ph), 130.6 (d, J_{CP} = 15.5 Hz, Ph), 130.4 (s, Ph), 130.2 (d, J_{CP} = 10.3 Hz, Ph), 129.9 (s, Ph), 129.8 (d, J_{CP} = 10.3 Hz, Ph), 128.0 (d, J_{CP} = 12.0 Hz, Ph), 83.9 (s, Cp), 68.7 (s, CH₂), 64.3 (s, CH₂); $^{31}P\{^1H\}$ 66.8 (s).

HRMS calc. for $C_{27}H_{23}NO_2P^{56}Fe$ 480.8015, found 480.8023; MS (FAB, 3-NBA, m/z) [27] 480 ([**11a**]⁺, 45%), 452 ([**11a**−CO]⁺, 55%); IR (cm⁻¹, neat) $\nu_{C≡O}$ 1971 (s), $\nu_{C=N}$ 1610 (m).

5.3.2. Synthesis of "[CpFe(CO)(7b)][I] · (CH₂Cl₂)", [11b][I] · (CH₂Cl₂)

PHOX **7b** (0.117 g, 0.327 mmol), CpFe(CO)₂I (0.090 g, 0.296 mmol) in toluene (1.5 mL) were reacted and worked up as described above for [**11a**][I]. Complex [**11b**][I] · (CH₂Cl₂) was isolated as a red solid (0.100 g, 0.139 mmol, 47%), m.p. 180–182 °C dec. (capillary). Anal. Calc. for $C_{29}H_{27}FeINO_2P \cdot (CH_2Cl_2)$: C, 50.03; H, 4.06. Found: C, 50.09; H, 4.04%.

NMR (δ, CDCl₃) ^1H 8.52–8.35 (m, 1H, Ph), 7.88–7.19 (m, 11H, Ph), 7.17–6.98 (m, 2H, Ph), 5.27 (CH₂Cl₂), 4.89 (s, 6 H, Cp + CHH′), 4.07 (d, J_{HH} = 8.4 Hz, 1H, CHH′), 1.34 (s, 3H, CH₃), 0.10 (s, 3H, CCH′₃); $^{13}C\{^1H\}$ 219.2 (d, J_{CP} = 29.4 Hz, CO), 167.4 (d, J_{CP} = 7.0 Hz, C=N), 134.7 (d, J_{CP} = 11.5 Hz, Ph), 133.6 (d, J_{CP} = 7.2 Hz, Ph), 133.3 (d, J_{CP} = 7.2 Hz, Ph), 132.7 (s, Ph), 132.5 (s, Ph), 132.5 (s, Ph), 132.3 (s, Ph), 131.8 (s, Ph), 131.6 (d, J_{CP} = 11 Hz, Ph), 131.3 (s, Ph), 130.9 (d, J_{CP} = 2.2 Hz, Ph), 130.5 (d, J_{CP} = 11.0 Hz, Ph), 129.6 (d, J_{CP} = 11.0 Hz, Ph), 129.1 (d, J_{CP} = 10.5 Hz, Ph), 128.7 (s, Ph), 128.2 (s, Ph), 128.0 (s, Ph), 84.1 (s, Cp), 79.6 (s, CH₂), 71.3 (s, CH₂), 53.4 (CH₂Cl₂), 25.7 (s, CH₃), 24.4 (s, CH′₃); $^{31}P\{^1H\}$ 64.3 (s).

HRMS calc. for $C_{29}H_{27}NO_2P^{56}Fe$ 508.1129, found 508.1125; MS (FAB, 3-NBA, m/z) [27] 508 ([**11b**]⁺, 95%), 480 ([**11b**−CO]⁺, 100%); IR (cm⁻¹, neat) $\nu_{C≡O}$ 1944 (s), $\nu_{C=N}$ 1610 (m); UV–Vis (nm (ε, M⁻¹ cm⁻¹), CH₂Cl₂, 0.05 mM) 230 (36 080), 368 (2940).

5.3.3. Synthesis of "[CpFe(CO)(7c)][I] · (CH₂Cl₂)₀.₅", [11c][I] (CH₂Cl₂)₀.₅

PHOX **7c** (0.200 g, 0.456 mmol), CpFe(CO)₂I (0.125 g, 0.411 mmol) in toluene (1 mL) were reacted and worked up as described above for [**11a**][I]. Complex [**11c**][I] · (CH₂Cl₂)₀.₅ was isolated as a red solid (0.271 g, 0.358 mmol, 87%), m.p. 180–182 °C dec. (capillary). Anal. Calc. for $C_{29}H_{26}BrFeINO_2P(CH_2Cl_2)_{0.5}$, 46.83; H, 3.60. Found: C, 47.10; H, 3.73%.

NMR (δ, CD₂Cl₂) [28] ^1H 8.49 (s, 1H, Ph), 7.85–7.95 (m, 1H, Ph), 7.69–7.65 (m, 3H, Ph), 7.46–7.34 (m, 6H, Ph), 7.18–7.14 (m, 2H, Ph), 5.27 (CH₂Cl₂), 4.91 (s, 5H, Cp), 4.68 (d, J_{HH} = 8.1 Hz, 1H, CHH′), 4.20 (d, J_{HH} = 8.4 Hz, 1H, CHH′), 1.51 (s, 3H, CH₃), 0.09 (s, 3H, CH′₃); $^{13}C\{^1H\}$ 219.0 (d, J_{CP} = 28.7 Hz, CO), 166.5 (d, J_{CP} = 6.8 Hz, C=N), 136.8

(d, J_{CP} = 8.3 Hz, Ph), 136.1 (br, Ph), 135.1 (d, J_{CP} = 10.5 Hz, Ph), 133.0 (br, Ph), 132.3 (s, Ph), 132.2 (s, Ph), 131.9 (d, J_{CP} = 10.8 Hz, Ph), 131.5 (d, J_{CP} = 2.5 Hz, Ph), 131.0 (s, Ph), 130.5 (s, Ph), 130.0 (d, J_{CP} = 10.0 Hz, Ph), 129.6 (d, J_{CP} = 10.8 Hz, Ph), 128.4 (s, Ph), 127.8 (s, Ph), 127.0 (d, J_{CP} = 2.5 Hz, Ph), 84.3 (s, Cp), 80.8 (s, CH₂), 72.2 (s, CH₂), 26.0 (s, CH₃), 24.7 (s, CH′₃); $^{31}P\{^1H\}$ 64.4 (s).

HRMS calc. for $C_{29}H_{26}^{79}BrNO_2P^{56}Fe$ 586.0233, found 586.0253; MS (FAB, 3-NBA, m/z) [27] 586 ([**11c**]⁺, 60%), 558 ([**11c**−CO]⁺, 100%); IR (cm⁻¹, neat) $\nu_{C≡O}$ 1947 (s), $\nu_{C=N}$ 1613 (m); UV–Vis (nm (ε, M⁻¹ cm⁻¹), CH₂Cl₂, 0.05 mM) 230 (40 280), 368 (1320).

5.3.4. Synthesis of "[CpFe(CO)(7d)][I] · (CH₂Cl₂)", [11d][I] · (CH₂Cl₂)

PHOX **7d** (0.151 g, 0.375 mmol), CpFe(CO)₂I (0.126 g, 0.415 mmol) in toluene (1 mL) were reacted and worked up as described above for [**11a**][I]. Complex [**11d**][I] · (CH₂Cl₂) was isolated as a red solid (0.065 g, 0.0853 mmol, 21%), m.p. 187–189 °C dec. (capillary). Anal. Calc. for $C_{31}H_{32}FeIN_2O_2P \cdot (CH_2Cl_2)$: C, 50.36; H, 4.49. Found: C, 50.94; H, 4.75%.

NMR (δ, CD₂Cl₂) [28] ^1H 7.55–7.11 (m, 12 H, Ph), 6.77 (br s, 1H, Ph), 4.83 (br s, 6H, Cp + CHH′), 4.68 (d, J_{HH} = 8.1 Hz, 1H, CHH′), 4.10 (br s, 1H, CHH′), 3.17 (s, 6H, N(CH₃)₂), 1.48 (s, 3H, CCH₃), 0.05 (s, 3H, CCH′₃); $^{13}C\{^1H\}$ 219.1 (d, J_{CP} = 28.4 Hz, CO), 167.6 (d, J_{CP} = 6.5 Hz, C=N), 151.4 (s, C–N), 134.4 (s, Ph), 134.1 (d, J_{CP} = 11.2 Hz, Ph), 133.8 (s, Ph), 131.7 (s, Ph), 131.2 (d, J_{CP} = 10.0 Hz, Ph), 130.9 (s, Ph), 130.2 (s, Ph), 129.5 (s, Ph), 129.1 (d, J_{CP} = 10.0 Hz, Ph), 128.5 (d, J_{CP} = 10.5 Hz, Ph), 116.9 (br m, Ph), 113.7 (d, J_{CP} = 7.6 Hz, Ph), 113.5 (s, Ph), 112.9 (s, Ph), 84.1 (s, Cp), 79.5 (s, CH₂), 70.8 (s, C(CH₃)₂), 40.3 (s, N(CH₃)₂), 26.1 (s, CH₃), 24.1 (s, CH′₃); $^{31}P\{^1H\}$ 61.3 (s).

HRMS calc. for $C_{31}H_{32}N_2O_2P^{56}Fe$ 551.1551, found 551.1561; MS (FAB, 3-NBA, m/z) [27] 551 ([**11d**]⁺, 40%), 523 ([**11d**−CO]⁺, 100%); IR (cm⁻¹, neat) $\nu_{C≡O}$ 1951 (s), $\nu_{C=N}$ 1583 (m); UV–Vis (nm (ε, M⁻¹ cm⁻¹), CH₂Cl₂, 0.025 mM) 245 (49 280), 231 (48 840), 296 (19 520), 361 (7280).

5.3.5. Synthesis of "[CpFe(CO)(7e)][I]", [11e+11e′][I]

PHOX **7e** (0.200 g, 0.474 mmol) and CpFe(CO)₂I (0.159 g, 0.524 mmol) in toluene (2 mL) were reacted and worked up as described above for [**11a**][I]. [**11e+11e′**][I] was isolated as mixture of diastereomers as a red solid (0.250 g, 0.359 mmol, 76%).

NMR (δ, CDCl₃) ^1H 8.09 (m, 1H, Ph), 7.70–7.48 (m, 8H, Ph), 7.37–7.21 (m, 5H, Ph), 7.06–6.94 (m, 3H, Ph), 6.85 (d, J_{HH} = 10.5 Hz, 1H, Ph), 5.86–5.81 (m, 1H, CH), 5.00–4.98 (m, 1H, CH), 4.61 (s, 5H, Cp), 4.19–4.14 (m, CH); $^{13}C\{^1H\}$(partial) 84.8 (s, Cp), 84.0 (s, Cp′); $^{31}P\{^1H\}$ 66.5 (s), 65.2 (s).

HRMS calc. for $C_{34}H_{29}NO_2P^{56}Fe$ 570.1284, found 570.1271; MS (FAB, 3-NBA, m/z) [27] 570 ([**11e**]⁺, 60%), 542 ([**11e**−CO]⁺, 100%); IR (cm⁻¹, neat) $\nu_{C≡O}$ 1950 (s), $\nu_{C=N}$ 1608 (m).

5.3.6. Synthesis of "[CpFe(CO)((R)-7f)][I]", [11f][I]

PHOX (R)-**7f** (0.344 g, 0.844 mmol) and CpFe(CO)₂I (0.230 g, 0.757 mmol) in toluene (2 mL) were reacted and worked up as described above for [**11a**][I]. Complex [**11f**][I] was isolated as a red solid (0.325 g, 0.476 mmol, 63%), m.p. 201–202 °C dec. (capillary). Anal. Calc. for $C_{33}H_{27}FeINO_2P$: C, 58.01; H, 3.98. Found: C, 57.74; H, 3.99%.

NMR (δ, CDCl₃) ^1H 8.09 (m, 1H, Ph), 7.70–7.48 (m, 8H, Ph), 7.37–7.21 (m, 5H, Ph), 7.06–6.94 (m, 3H, Ph), 6.85 (d, J_{HH} = 10.5 Hz, 1H, Ph), 5.86–5.81 (m, 1H, CH), 5.00–4.98 (m, 1H, CH), 4.61 (s, 5H, Cp), 4.19–4.14 (m, 1H, CH); $^{13}C\{^1H\}$ 216.9 (d, J_{CP} = 27.3 Hz, CO), 167.7 (d, J_{CP} = 4.7 Hz, C=N), 139.9 (s, Ph), 133.7 (d, J_{CP} = 6.5 Hz, Ph), 132.9 (s, Ph), 132.72 (s, Ph), 132.68 (s, Ph), 132.5 (s, Ph), 132.2 (s, Ph), 132.14 (s, Ph), 132.11 (s, Ph), 131.9 (d, J_{CP} = 3.0 Hz, Ph), 131.2 (s, Ph), 130.9 (s, Ph), 130.6 (s, Ph), 130.4 (d, J_{CP} = 6.2 Hz, Ph), 129.8 (d, J_{CP} = 10.0 Hz, Ph), 129.6 (d, J_{CP} = 10.6 Hz, Ph), 129.1 (s,

Ph), 128.4 (s, Ph), 127.5 (d, J_{CP} = 10.8 Hz, Ph), 126.6 (s, Ph), 82.7 (s, Cp), 76.5 (s, CH_2), 75.5 (s, CH_2); $^{31}P\{^1H\}$ 67.0.

HRMS calc. for $C_{33}H_{27}NO_2P^{56}Fe$ 556.1128, found 556.1125; MS (FAB, 3-NBA, m/z) [27] 556 ([**11f**]$^+$, 60%), 528 ([**11f**−CO]$^+$, 100%); IR (cm^{-1}, neat) $\nu_{C\equiv O}$ 1967 (s), $\nu_{C\equiv N}$ 1603 (s).

5.4. General procedures for counter ion exchanges

5.4.1. Synthesis of "[CpFe(CO)(7b)][ClO₄]", [11b][ClO₄]

A solution of $NaClO_4$ (0.144 g, 1.183 mmol) in MeOH (1.5 mL) was added dropwise to a solution of complex [**11b**][I] (0.150 g, 0.237 mmol) in MeOH (1.5 mL) with stirring. The reaction mixture was stirred for 30 min. A precipitate formed. The solvent was decanted, and the red solid residue washed with MeOH (3 × 1 mL). The residue was dried in high vacuum to obtain [**11b**][ClO₄] as red powder (0.085 g, 0.140 mmol, 59%).

NMR (δ, CD_2Cl_2) ^1H 8.17–8.11 (m, 1H, Ph), 7.82–7.46 (m, 7H, Ph), 7.41–7.20 (m, 6H, Ph), 7.12–7.02 (m, 2H, Ph), 4.71 (5H, Cp), 4.31 (d, J_{HH} = 8.5 Hz, 1H, CHH′), 4.11 (d, J_{HH} = 8.5 Hz, 1H, CHH′), 1.38 (s, 3H, CH_3), 0.01 (s, 3H, CCH_3'); $^{13}C\{^1H\}$ 167.8 (br, C≡N), 135.3 (d, J_{CP} = 11.3 Hz, Ph), 134.1 (d, J_{CP} = 7.0 Hz, Ph), 133.6 (s, Ph), 133.0 (d, J_{CP} = 2.5 Hz, Ph), 132.7 (s, Ph), 132.67 (s, Ph), 132.62 (s, Ph), 132.60 (s, Ph), 132.58 (s, Ph), 132.0 (d, J_{CP} = 10.7 Hz, Ph), 131.4 (d, J_{CP} = 3.0 Hz, Ph), 130.6 (s, Ph), 130.0 (s, Ph), 129.9 (s, Ph), 129.6 (d, J_{CP} = 10.4 Hz, Ph), 129.2 (d, J_{CP} = 1.0 Hz, Ph), 128.8 (s, Ph), 84.2 (s, Cp), 80.0 (s, CH_2), 71.9 (s, CH_2), 26.3 (s, CH_3), 24.6 (s, CH_3'); $^{31}P\{^1H\}$ 64.6 (s).

HRMS calc. for $C_{29}H_{27}NO_2P^{56}Fe$ 508.1129, found 508.1115; MS (FAB, 3-NBA, m/z) [27] 508 ([**11b**]$^+$, 50%), 480 ([**11b**−CO]$^+$, 100%); IR (cm^{-1}, neat) $\nu_{C\equiv O}$ 1958 (s), $\nu_{C\equiv N}$ 1622 (m).

5.4.2. Synthesis of "[CpFe(CO)(7f)][PF₆]", [11f][PF₆]

$NaPF_6$ (0.037 g, 0.219 mmol) in MeOH (1.5 mL) was reacted with [CpFe(CO)(**7e**)][I] (0.030 g, 0.044 mmol) in MeOH (1.5 mL) and worked up as described above for [**11b**][ClO₄] to obtain [**11f**][PF₆] as red powder (0.025 g, 0.036 mmol, 81%).

NMR (δ, CD_2Cl_2) ^1H 8.09–8.01 (m, 1H, Ph), 7.72–6.91 (m, 16H, Ph), 6.68–6.54 (m, 1H, Ph), 4.97–4.80 (m, 1H, CH), 4.80–4.70 (m, 1H, CH), 4.41 (s, 5H, Cp), 4.27–4.12 (m, 1H, CH); $^{31}P\{^1H\}$ 65.7 (s, PPh₂); −143.7 (qintet, J_{PF} = 710 Hz, PF₆).

HRMS calc. for $C_{33}H_{27}NO_2P^{56}Fe$ 556.1128, found 556.1125; MS (FAB, 3-NBA, m/z) [27] 556 ([**11f**]$^+$, 60%), 528 ([**11f**−CO]$^+$, 100%); IR (cm^{-1}, neat) $\nu_{C\equiv O}$ 1967 (s), $\nu_{C\equiv N}$ 1604 (m).

5.5. X-ray structure determination of [11a][I], [11b][ClO₄], [11c][I], [11d][I] and [11f][PF₆]

To obtain X-ray quality crystals, CH_2Cl_2 solutions of [**11a**][I], [**11c**][I], and [**11f**][PF₆], an acetone solution of [**11b**][ClO₄] and a $CHCl_3$ solution of [**11d**][I] were layered with Et_2O and stored for 18 h at −18 °C.

Data collections were performed as outlined in Table 2 using a Bruker Kappa Apex II Charge Coupled Device (CCD) Detector system single crystal X-ray diffractometer equipped with an Oxford Cryostream LT device. Preliminary unit cell constants were determined with a set of 36 narrow frame scans. Collected data were corrected for systematic errors using SADABS [29a]. Crystal data and intensity data collection parameters are listed in Table 2. Structure solution and refinement were carried out using the SHELXTL-PLUS software package [29b]. The structures were solved by direct methods and refined successfully in the space groups listed in Table 2, and special details of refinement are as follows. Complex [**11a**][I]: The lattice contains a molecule of disordered CH_2Cl_2. Disordered Cl atoms were resolved with partial occupancies of 60:40%. Complex [**11c**][I]: Due to very weak and poor quality data several atoms resulted in non positive definite

(NPD) anisotropic thermal parameters. These were refined with EADP (SHELX-TL) restraints. Complex [**11d**][I]: There are two unique molecules in the asymmetric unit for this compound. The lattice contains several solvent molecules. A total of four molecules of $CHCl_3$, a molecule of Et_2O and two molecules of H_2O (one full and two half molecules) were located and refined. Of the four $CHCl_3$, Cl atom disorders were resolved with partial occupancies for two solvates. Complex [**11f**][PF₆]: The molecule exhibits large amount of disorder. Several phenyl motifs have more than one orientations. These were modeled using SAME and EADP (SHELX-TL) restraints.

5.6. Cyclic voltammetry

The voltammograms were recorded with a Princeton Applied Research Parstat 2273 Electrochemical System and analyzed with POWERSUITE 2.58 software. Cells were fitted with a glassy carbon working electrode, and an Ag wire pseudoreference electrode and a platinum wire as auxiliary electrode. All CH_2Cl_2 solutions were 2×10^{-3} M in substrate and 0.05 M in n-$Bu_4N^+PF_6^-$ and degassed with argon. All cyclic voltammograms were recorded with a scan rate of 100 mV s^{-1}. Ferrocene was subsequently added, and calibration voltammograms recorded. All potentials are references to the observed $E_{1/2}$ value for the ferrocene/ferrocenium couple. The ambient laboratory temperature was 22 ± 1 °C.

Appendix A. Supplementary material

CCDC 689550, 689549, 689547, 689546 and 689548 contain the supplementary crystallographic for [**11a**][I], [**11b**][ClO₄], [**11c**][I], [**11d**][I] and [**11f**][PF₆]. These data can be obtained free of charge from The Cambridge Crystallographic Data Centre via www.ccdc.cam.ac.uk/data_request/cif.

Supplementary data (experimental details and NMR data (^1H, ^{13}C, ^{19}F) for compounds **3**, **4**, **5**, **6**, **8**, **9**, and **10**; cyclic voltammograms) associated with this article can be found, in the online version, at doi:10.1016/j.jorganchem.2008.06.031.

References

[1] (a) G. Helmchen, A. Pfaltz, Acc. Chem. Res. 33 (2000) 336;
   (b) H.A. McManus, P.J. Guiry, Chem. Rev. 104 (2004) 4151.
[2] (a) P. von Matt, A. Pfaltz, Angew. Chem., Int. Ed. Engl. 32 (1993) 566;
   (b) J. Sprinz, G. Helmchen, Tetrahedron Lett. 34 (1993) 1769;
   (c) G.J. Dawson, C.G. Frost, J.M. Williams, S.J. Coote, Tetrahedron Lett. 34 (1993) 3149.
[3] R. Crabtree, Acc. Chem. Res. 12 (1979) 331.
[4] (a) F.M. Geisler, G. Helmchen, J. Org. Chem. 71 (2006) 2486;
   (b) C. García-Yebra, J.P. Jannsen, F. Rominger, G. Helmchen, Organometallics 23 (2004) 5459;
   (c) M. Zehnder, S. Schaffner, M. Neuburger, D.A. Plattner, Inorg. Chim. Acta 337 (2002) 287;
   (d) G. Helmchen, J. Organomet. Chem. 576 (1999) 203;
   (e) M. Ogasawara, K. Yoshida, H. Kamei, K. Kato, Y. Uozumi, T. Hayashi, Tetrahedron: Asymmetry 9 (1998) 1779;
   (f) J.P. Jannsen, G. Helmchen, Tetrahedron Lett. 38 (1997) 8025.
[5] J.A. Keith, D.C. Behenna, J.T. Mohr, S. Ma, S.C. Marinescu, J. Oxgaard, B.M. Stoltz, W.A. Goddard III, J. Am. Chem. Soc. 129 (2007) 11876.

[6] (a) O. Loiseleur, M. Hayashi, M. Keenan, N. Schmees, A. Pfaltz, J. Organomet. Chem. 576 (1999) 16;
(b) O. Loiseleur, M. Hayashi, N. Schmees, A. Pfaltz, Synthesis 11 (1997) 1338.

[7] (a) S. Bell, B. Wüstenberg, S. Kaiser, F. Menges, T. Netscher, A. Pfaltz, Science 311 (2006) 642;
(b) D. Liu, W. Tang, X. Zhang, Org. Lett. 6 (2004) 513;
(c) A. Lightfoot, P. Schnider, A. Pfaltz, Angew. Chem., Int. Ed. 37 (1998) 2897.

[8] F. Naud, C. Malan, F. Spindler, C. Rüggeberg, A.T. Schmidt, H.U. Blaser, Adv. Synth. Catal. 348 (2006) 47.

[9] T. Langer, G. Helmchen, Tetrahedron Lett. 37 (1996) 1381.

[10] (a) D. Ca, C. Vega, N. García, F.J. Lahoz, S. Elipe, L.A. Oro, M.P. Lamata, F. Viguri, R. Borao, Organometallics 25 (2006) 1592;
(b) D. Carmona, F.J. Lahoz, S. Elipe, L.A. Oro, M.P. Lamata, F. Viguri, F. Sánchez, S. Martínez, C. Cativiela, M.P. López-Ram de Víu, Organometallics 21 (2002) 5100;
(c) K. Hiroi, K. Watanabe, Tetrahedron: Asymmetry 13 (2002) 1841.

[11] E.L. Stangeland, T. Sammakia, Tetrahedron 53 (1997) 16503.

[12] H. Grützmacher, Angew. Chem., Int. Ed. 47 (2008) 1814.

[13] K. Tani, D.C. Behenna, R.M. McFadden, B.M. Stoltz, Org. Lett. 9 (2007) 2529.

[14] (a) C. Bolm, J. Legros, J. Le Paih, L. Zani, Chem. Rev. 104 (2004) 6217;
(b) M. Costas, M.P. Mehn, M.P. Jensen, L. Que Jr., Chem. Rev. 104 (2004) 939;
(c) E.Y. Tshuva, S.J. Lippard, Chem. Rev. 104 (2004) 987;
(d) A. Fürstner, R. Martin, Chem. Lett. 34 (2005) 624.

[15] (a) P. Braunstein, G. Clerc, X. Morise, New J. Chem. 27 (2003) 68;
(b) P. Braunstein, G. Clerc, X. Morise, R. Welter, G. Mantovani, Dalton Trans. (2003) 1601.

[16] J.A. Frump, Chem. Rev. 71 (1971) 483.

[17] (a) K. Katagiri, H. Danjo, K. Yamaguchi, T. Imamoto, Tetrahedron 61 (2005) 4701;
(b) J.V. Allen, G.J. Dawson, C.G. Frost, J.M.J. Williams, S.J. Coote, Tetrahedron 50 (1994) 799.

[18] M. Peer, J.C. de Jong, M. Kiefer, T. Langer, H. Rieck, H. Schell, P. Sennhenn, J. Sprinz, H. Steinhagen, B. Wiese, G. Helmchen, Tetrahedron 52 (1996) 7547.

[19] R.B. King, F.G.A. Stone, W.L. Jolly, G. Austin, W. Covey, D. Rabinovich, H. Steinberg, R. Tsugawa, Inorg. Synth. 7 (1963) 99.

[20] (a) A. Palazzi, S. Stagni, S. Bordoni, M. Monari, S. Selva, Organometallics 21 (2002) 3774;
(b) M.T. Ashby, J.H. Enemark, D.L. Lichtenberger, Inorg. Chem. 27 (1988) 191.

[21] (a) S. Nakanishi, K. Goda, S. Uchiyama, Y. Otsuji, Bull. Chem. Soc. Jpn. 65 (1992) 2560;
(b) N. Coville, E.A. Darling, A.W. Hearn, P. Johnston, J. Organomet. Chem. 328 (1987) 375;
(c) P. Vierling, J.G. Riess, A. Grand, Inorg. Chem. 25 (1986) 4144.

[22] (a) M. Kollmar, G. Helmchen, Organometallics 21 (2002) 4771;
(b) M. Kollmar, B. Goldfuss, M. Reggelin, F. Rominger, G. Helmchen, Chem. Eur. J. 7 (2001) 4913.

[23] (a) R.S. Cahn, C. Ingold, V. Prelog, Angew. Chem., Int. Ed. Engl. 5 (1966) 385;
(b) K. Stanley, M.C. Baird, J. Am. Chem. Soc. 97 (1975) 6598.

[24] Determination of the optical rotation from a solution with $c = 0.1$ gave a $[\alpha]_D^{26}$ value of +12, but it fluctuated too heavily for an accurate reproduction.

[25] W.E. Geiger, in: P.T. Kissinger, W.R. Heinemann (Eds.), Laboratory Techniques in Electroanalytical Chemistry, Marcel Dekker, New York, 1996, p. 684.

[26] M.M. Rahmann, H.-Y. Liu, K. Eriks, A. Prock, W.P. Giering, Organometallics 8 (1989) 1.

[27] The most intense peak of isotope envelope (relative intensity, %) are listed.

[28] The CH_2Cl_2 solvate molecules were detected in corresponding $CDCl_3$ spectra, which were, due to poor solubility, of poorer quality.

[29] (a) R.H. Blessing, Acta Crystallogr., Sect. A 51 (1995) 33;
(b) G.M. Sheldrick, Acta Crystallogr., Sect. A 64 (2008) 112.